

High-speed spiral nan positioning

Andreas Kotsopoulos^{*,*} Angeliki Pantazi^{**} Abu Sebastian^{**}
Theodore Antonakopoulos^{*}

^{*} Dept. of Electrical and Computers Engineering, University of Patras,
26500, Rio-Patras, Greece, (e-mail: akotsop, antonako@upatras.gr).

^{**} IBM Research - Zurich, Rüschlikon, CH-8803, Switzerland, (e-mail:
agp, ase@zurich.ibm.com).

Abstract: Nanometer-precise positioning at ultra-high velocities is a major challenge for rapidly emerging applications that use scanning probes in order to observe and alter the properties of materials down to the nanoscale. Typical examples include surface imaging, nanolithography and data storage. For example in probe-based data storage, constant linear velocity along the scan trajectory is required, in order for storage operations to be feasible. In this paper, a spiral-enhanced tracking control architecture is presented for the constant linear velocity spiral case. The proposed controller exploits the spire-wise narrowband frequency content of the reference signal, enabling very high speed and accurate positioning. The tracking performance and high-frequency operation are corroborated with experimental results from a piezo-actuated nanopositioner with magneto-resistance-based position sensors.

Keywords: spiral, nan positioning, H_∞ , high-speed, peak filter.

1. INTRODUCTION

During the last few years, rapidly emerging scanning probe based applications, such as biological sample imaging, nanolithography, and probe-based data storage, have posed a major challenge for prospective control schemes in order for combined high-speed and high-precision positioning to become feasible [see Shibata et al. (2010), Mishra et al. (2007), Pantazi et al. (2007), Sebastian et al. (2008)]. In such systems, nan positioning scanners, based on Micro-Electro-Mechanical-Systems (MEMS) or piezoelectric elements, with x/y-axis displacement capabilities are used for accurate positioning of the sample with respect to a probe or an array of parallel operating probes equipped with nanometer-sharp tips [see Devasia et al. (2007)].

Most of today's scanning probe systems [see for instance Pantazi et al. (2008) and Bhushan (2004)], drive the nanopositioner along a raster or similar trajectory, which can be generated with a triangular-shaped waveform and a staircase or ramp waveform in its fast and slow scan axis respectively. Nevertheless, the existence of abrupt changes in direction, produces undesired oscillations and widens the bandwidth of the reference signal. Moreover, during backward motion towards the start of the next line to be scanned readback is usually suspended, resulting in intermittent system operation. The aforementioned properties significantly limit the achievable scan speed and system data rate. One way to overcome these issues is by applying alternative scanning schemes with desirable smoothness and continuity properties. A scanning scheme has been recently introduced and analyzed for the case of probe-based data storage and nan positioning [see Kotsopou-

los and Antonakopoulos (2010)]. The scheme is based on archimedean spiral scan trajectories and allows for fixed-step high-speed perpetual scanning operation.

In this work, an H_∞ based control architecture enhanced with a frequency sliding peak filter structure is presented. The architecture exploits the inherent characteristics of the spiral reference signal, in order to improve the spire-wise tracking capability of the feedback loop. It is demonstrated, that the combined architecture outperforms the standalone H_∞ controller, resulting in high quality tracking even at scan frequencies beyond 1000 Hz. Furthermore, it is shown, that by using the proposed architecture, a low bandwidth H_∞ controller can be used instead of a high bandwidth H_∞ controller, yielding similar results in terms of tracking performance, while the system's susceptibility to measurement noise is decreased. The tracking performance of both schemes is experimentally corroborated by applying them on a fast piezoelectrically actuated nanopositioner recently published in Kartik et al. (2010). Related work in the contexts of constant linear and constant angular spiral nan positioning and imaging applications can be found in Mahmood and Moheimani (2009), Kotsopoulos et al. (2010) and Mahmood et al. (2011).

The rest of this paper is organized as follows. In Section 2 we provide a brief description of the piezoscanner system, while in Section 3 the general control architecture, as well as the high and low bandwidth controller design procedure and analysis are presented. Section 4 describes the experimental setup used and presents experimental results that verify the advantages of the proposed scheme. Finally, in Section 5 we summarize and provide our conclusions from this work.

^{*} Andreas Kotsopoulos is currently (Aug. 2010 - Oct. 2010) with the IBM Research - Zurich, Rüschlikon, CH-8803, Switzerland.

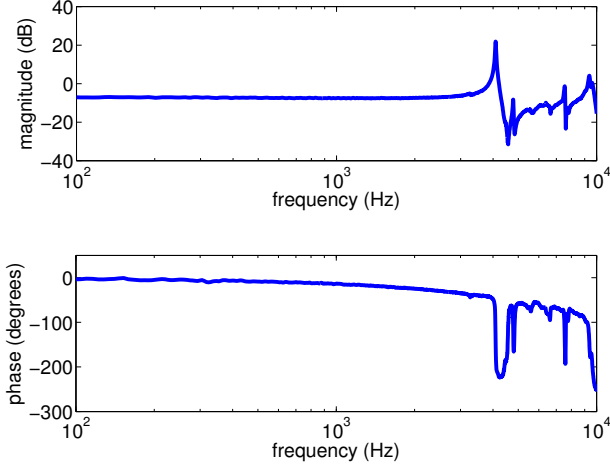


Fig. 1. Experimentally obtained frequency response of the scanner in the x-axis using the GMR position sensors.

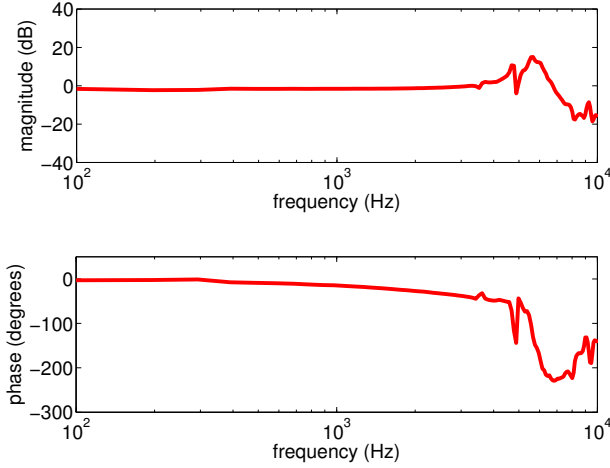


Fig. 2. Experimentally obtained frequency response of the scanner in the y-axis using the GMR position sensors.

2. SYSTEM DESCRIPTION

The system under consideration comprises a scanner with x/y-plane displacement capabilities, based on two piezoelectric actuators with approximately $4 \mu\text{m}$ and $8 \mu\text{m}$ travel range in the x and y axis respectively. Position information is provided by a pair of Giant-Magneto-Resistance (GMR) based sensing elements [see for instance Daughton (2003) and Sahoo et al. (2011)], one for each axis of motion. The measurement noise introduced by the GMR sensors is dominated by $1/f$ noise. The standard deviation of the integrated noise from the GMR sensors over a range of 10 kHz was found to be 2.36 nm. The experimentally obtained frequency responses of the system using the position sensors are depicted in Fig. 1 for the x-axis and in Fig. 2 for the y-axis. Due to the high rigidity flexures and the low carried mass, the scanner presents a very high bandwidth with an almost flat response until the first resonances, which appear at 4.1 kHz and 4.77 kHz in the x and y axis respectively.

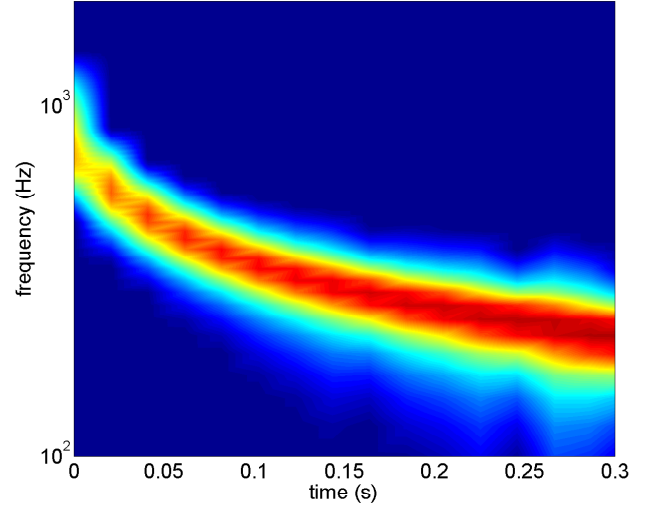


Fig. 3. Spectrogram of x-axis spiral reference signal.

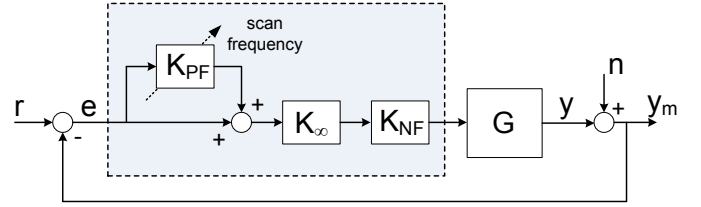


Fig. 4. Block diagram of general control architecture.

3. CONTROLLER DESIGN

In each individual axis, the constant linear velocity archimedean spiral reference signal can be seen in the time domain as a very narrowband frequency-shifting signal with varying magnitude. This is better understood by Fig. 3, showing the x-axis signal spectrogram of a representative spiral reference case. Furthermore, the way that both the center frequency and the frequency range of the signal depend on the instant spiral radius for a given constant linear velocity can be a priori calculated, and appropriately exploited by the controller for increased spiral tracking efficiency.

Two individual controllers with identical architecture were used for the control of the nanopositioner, one for each axis of motion. The proposed control architecture is depicted in the block diagram of Fig. 4. The feedback loop comprises a frequency-sliding peak filter structure, an H_∞ controller denoted by K_∞ , and a pair of notch filters denoted by K_{NF} , all connected in a cascade manner. Two different H_∞ controllers were designed and implemented for the evaluation of the architecture in terms of tracking performance, a high bandwidth, and a low bandwidth controller with the advantage of decreased susceptibility to measurements noise.

For the design of the K_∞ , the H_∞ control framework was used. The problem formulation according to the framework is shown in Fig. 5. Sixth-order transfer function fits capable of capturing the first two resonances of the plant were used in the H_∞ synthesis process, yielding eighth-order controllers in both cases (high and low bandwidth).

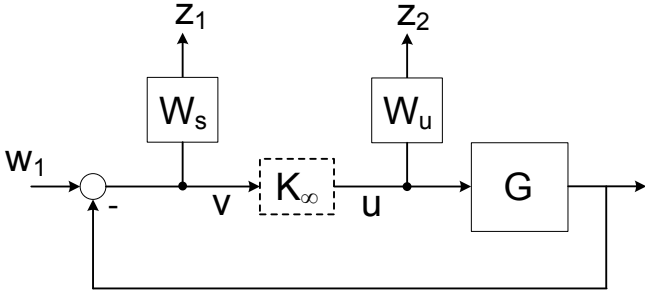


Fig. 5. Problem formulation of one-degree-of-freedom H_∞ controller design.

The shaping specifications for the closed loop transfer functions were expressed through the weighting functions W_s and W_u shown in Fig. 6, capturing the requirements on tracking performance and control effort limits respectively. Finally, v and u denote the input to the controller and the controlled output respectively, while $w = [w_1]$ the “exogenous input” signal vector and $z = \begin{bmatrix} z_1 \\ z_2 \end{bmatrix}$ the “exogenous output” signal vectors. The system can then be described as:

$$\begin{bmatrix} z_1 \\ z_2 \\ v \end{bmatrix} = P \cdot \begin{bmatrix} w_1 \\ u \end{bmatrix}, \quad u = K_\infty v \quad (1)$$

where P denotes the generalized plant given by:

$$P = \begin{bmatrix} W_s & -W_s G \\ 0 & W_u \\ 1 & -G \end{bmatrix} \quad (2)$$

The closed loop transfer function matrix T_{zw} relating z with w is the linear fractional transformation of K_∞ around P , given by:

$$T_{zw} = F_l(P, K_\infty) = \begin{bmatrix} \frac{W_s}{1 + GK_\infty} \\ \frac{W_u K_\infty}{1 + GK_\infty} \end{bmatrix} \quad (3)$$

The H_∞ control problem is then that of finding a stabilizing controller K_∞ such that $\|T_{zw}\|_\infty < \gamma_\infty$, where γ_∞ a constant approximately equal to 1 [Skogestad and Postlethwaite (2005)].

The peak filter can be constructed according to:

$$K_{PF}(s) = \frac{s^2 + 2\zeta_1\omega_c s + \omega_c^2}{s^2 + 2\zeta_2\omega_c s + \omega_c^2} \quad (4)$$

where $f_c = \omega_c/(2\pi)$ denotes the sliding frequency of the filter’s peak-magnitude point, and ζ_1, ζ_2 the damping ratios of the filter. The peak frequency f_c shifts continuously in time, adjusting to the corresponding shift of the center scan frequency along the spiral trajectory. Its value at the time instants determined by the filter coefficient update rate can be calculated in advance as a function of the spiral radius along the trajectory [see Kotsopoulos et al. (2010)].

The damping ratios ζ_1 and ζ_2 can be directly expressed with respect to the parameters M, N, Δ as:

$$\zeta_1 = \frac{\Delta^2 + 2\Delta}{2(1 + \Delta)} \sqrt{(10^{N/20})^2 - 1}, \quad \zeta_2 = \frac{\zeta_1}{10^{M/20}} \quad (5)$$

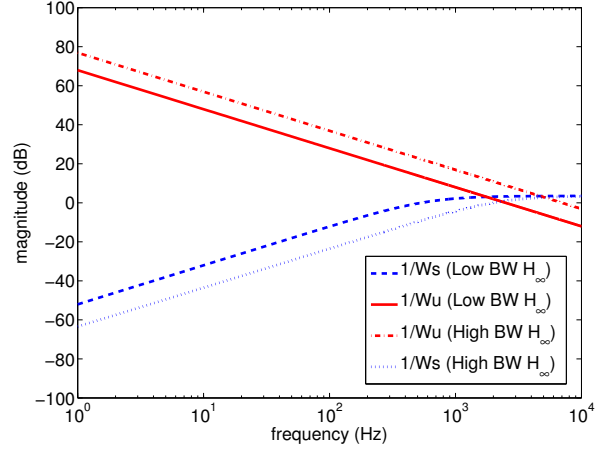


Fig. 6. Weighting transfer functions for the H_∞ designs.

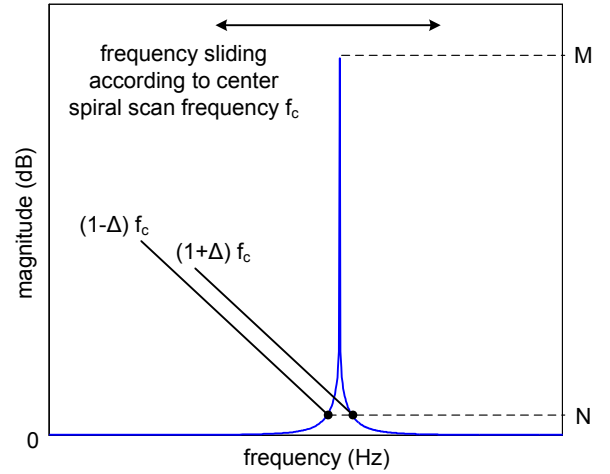


Fig. 7. Peak filter design and parameterization.

The parameters M, N, Δ are selected according to the desired magnitude response of the filter, and are illustrated qualitatively in Fig. 7. Specifically, M denotes the magnitude in dB at f_c , and N the magnitude in dB at the frequency points around the f_c , which are determined by the value of the variation Δ . For a more thorough and general analysis of peak filters see for example Mamun et al. (2007) and the related references therein.

Finally, in order to compensate for and prevent from overly exciting the higher order resonances, which are not included in the sixth-order transfer function models, a pair of notch filters denoted by K_{NF} were used. The resulting x-axis sensitivity (denoted by S) transfer function, relating the reference input with the tracking error signal, and complementary sensitivity (denoted by T_{yr}) transfer function, relating the reference with the output, are depicted in Fig. 8 for the high and low bandwidth designs and without the peak filter included in the loop. In Fig. 9, three time snapshots of the sensitivity transfer function for the high bandwidth H_∞ case when the peak filter is included in the loop are illustrated. The corresponding spiral scan frequencies are 100 Hz, 500 Hz and 1300 Hz (randomly selected in the scan frequency range of interest).

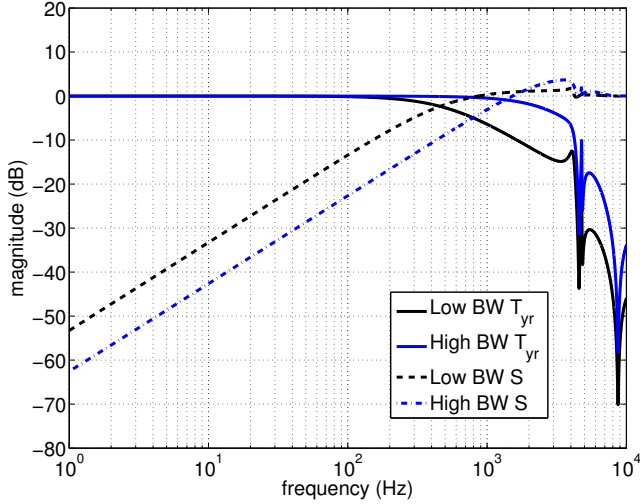


Fig. 8. Comparison of x-axis closed loop transfer functions for high and low bandwidth H_∞ designs without the peak filter included in the loop.

It can be seen that the insertion of any of the peak filters corresponding to a particular frequency does not compromise the stability of the closed loop system. Moreover, the closed loop system exhibits good stability margins. We believe that this, along with the fact that the filter coefficients are varying smoothly (inherently smooth spiral motion) and slowly (proper filter coefficients update rate selection) in time, ensures the stability of the closed loop system during the spiral scan operation. A more thorough stability analysis is a subject of future work.

In closed form the transfer functions of the combined architecture can readily be calculated as:

$$T_{yr} = \frac{(1 + K_{PF})K_\infty K_{NFG}}{1 + (1 + K_{PF})K_\infty K_{NFG}} \quad (6)$$

$$S = \frac{1}{1 + (1 + K_{PF})K_\infty K_{NFG}} \quad (7)$$

Note also, that for a fair comparison between the cases where the peak filters are activated or deactivated in the loop, the gain of the K_∞ has to be reduced by half in order to offset the gain introduced by the peak filter structure. The bandwidth of the closed loop system, determined by the frequency point at which the sensitivity function crosses the -3 dB point from below, is approximately 400 Hz for the low bandwidth and 1 kHz for the high bandwidth controllers, which shows that the requirements imposed by the first-order weighting functions at the design stage were well met. In both cases, a significant drop in the sensitivity transfer function at the frequency where the peak filter acts is evident.

4. EXPERIMENTAL RESULTS

The controllers were implemented in a digital signal processor using a sampling frequency of 100 kHz. The update rate of the peak filter's coefficients was set to 8 positioning instants. The performance evaluation of the proposed controller architecture in terms of tracking was based on the measured position information available from the x/y

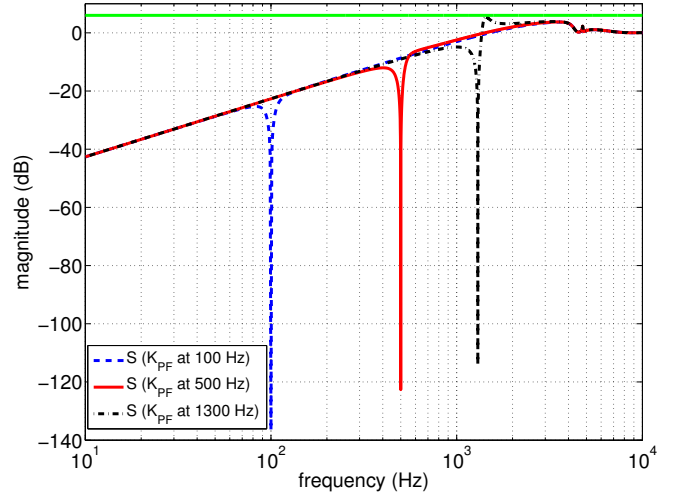


Fig. 9. x-axis time snapshots of the sensitivity transfer function for the high bandwidth H_∞ design case with the peak filter acting at 100 Hz, 500 Hz and 1300 Hz.

GMR position sensors, as well as on the achieved imaging quality of a nanofabricated medium sample. The imaging sample used was an island-shaped nanoscale pattern on silicon wafer measuring approximately 1.1 μm , 260 nm and 100 nm in the x, y and z axis respectively.

Aggregated comparative experimental results are presented in Fig. 10. The first figure set (1a-c) corresponds to the high bandwidth H_∞ controller and a constant linear velocity of 0.2 nm/ μs , while the spire pitch is 20 nm. The second figure set (2a-c) corresponds to the low bandwidth H_∞ controller for the same constant linear velocity and spire pitch. Finally, the third figure set (3a-c) corresponds to the low bandwidth H_∞ controller for a constant linear velocity of 0.75 nm/ μs and a spire pitch of 10 nm. In the high bandwidth H_∞ controller design case (see Figure 9 (1a-c)), the inclusion of the peak filter leads to reduced tracking error with respect to the case when only the K_∞ component is used. This can be seen clearly in the x/y position error, but also from a comparison of the image quality near the high frequency center region of the two obtained images.

Moreover, achieving accurate tracking of high frequency reference signals usually requires high bandwidth controller designs. However, this approach leads in most cases to an increase in the system's sensitivity to measurement noise due to the integration of sensor noise over a broader frequency region. A direct comparison between the result sets (1a-c) corresponding to the high bandwidth and (2a-c) corresponding to the low bandwidth of Fig. 10, verifies that the introduction of the peak filter structure, for enhanced tracking at only the spire-determined narrowband frequency region of interest, enables the use of a low bandwidth controller with less than half the bandwidth of the high bandwidth design, yielding similar tracking performance. This is evident from the similar quality in the obtained images (1b and 2b) as well as from the corresponding x/y position errors (1c and 2c). Nevertheless, as previously stated, using a low bandwidth design results in a reasonable decrease in the closed loop system's sus-

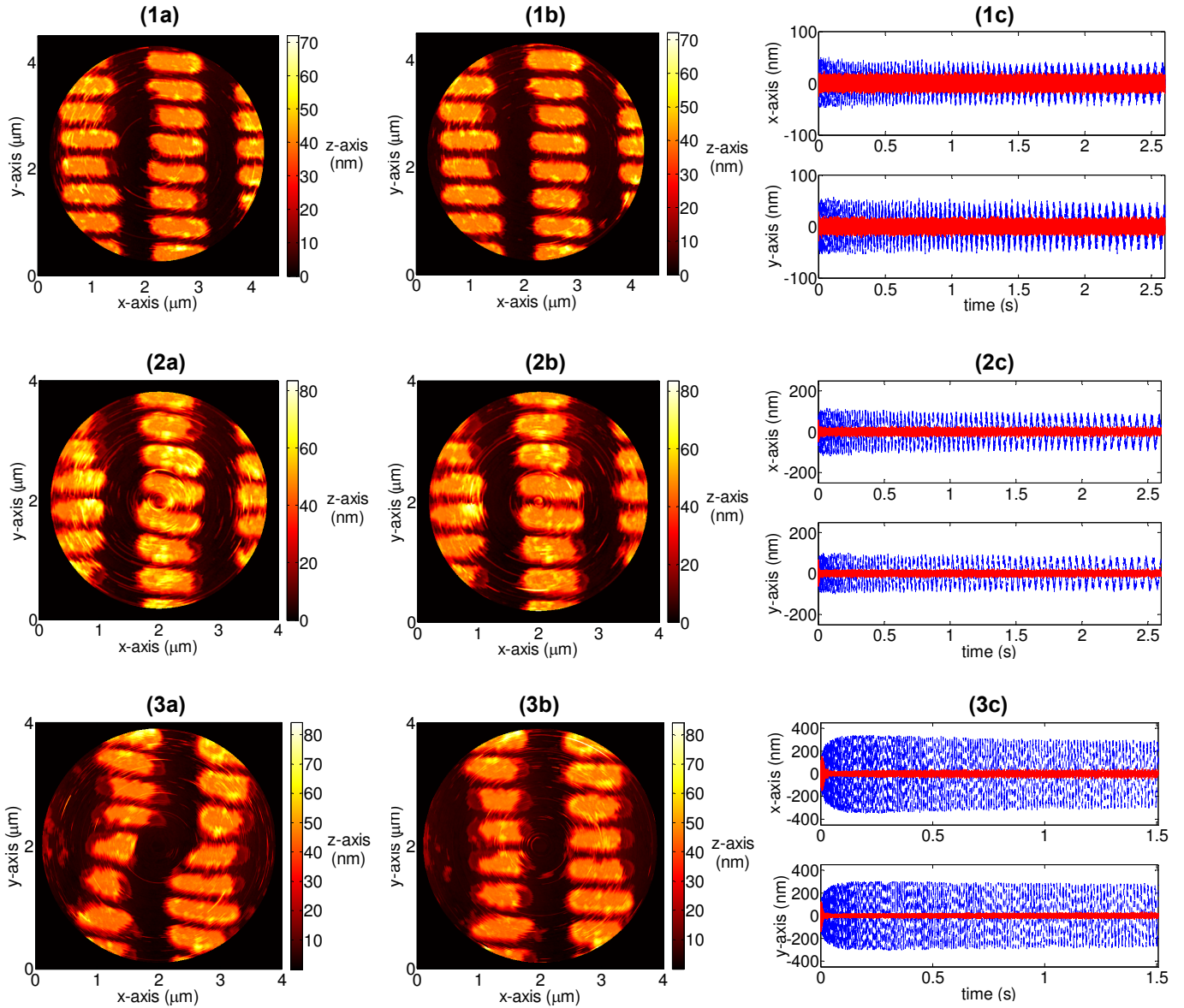


Fig. 10. Experimentally obtained images of a nanoscale structure on silicon wafer with approximately $1.1 \mu\text{m}$ (length) \times 260 nm (width) \times 100 nm (height) islands placed at fixed distances. Figures (a)-(b): Images obtained at closed loop operation without the peak filters and with the peak filters included in the control loop, respectively. Figures (c) shows the position tracking error for the two cases (blue dashed line: without peak filters, red solid line: with peak filters). Figure set (1): High bandwidth H_∞ controller. The corresponding constant linear velocity is $0.2 \text{ nm}/\mu\text{s}$. The reference signal is an archimedean spiral with a spire pitch of 20 nm . Figure set (2): Low bandwidth H_∞ controller. The corresponding constant linear velocity is $0.2 \text{ nm}/\mu\text{s}$ and the spire pitch is set to 20 nm . Figure set (3): Low bandwidth H_∞ controller. The constant linear velocity is set to $0.75 \text{ nm}/\mu\text{s}$ and the distance between successive spires to 10 nm .

ceptibility to measurement noise. Notice also the greater improvement in the image quality in (2b), where the peak filter is activated, relative to the case when the peak filter is deactivated (2a).

In the last case where the linear velocity is almost quadruple (3a-c), the aforementioned improvement is even greater, which is expected given the only 400 Hz bandwidth of the closed loop system. It should be noted that the imperfections of the island pattern in the surface region shown in the images are arising from the manufacturing process and are not a result of tracking error.

Finally, the transient response of the system is not investigated in terms of the time required for the system to reach steady state, since this property depends highly on the selected approach/seek procedure, which is outside the scope of this work.

5. CONCLUSIONS

In this work a control architecture based on the H_∞ control design framework was presented. The proposed controller's characteristics are such that the inherent properties of spiral nanopositioning signals are exploited, in

order for accurate tracking of high-frequency inputs to be achieved. For this purpose, the feedback loop has been extended with peak filters that shift smoothly in frequency in such a way, that an additional tracking gain is provided only at the instantaneous spiral scan frequency of interest, which can be a priori known to the controller. Additionally, it has been shown that by using the proposed combined scheme, a low bandwidth H_∞ with low sensitivity to measurement noise can be used instead, without significant tracking performance degradation. In each case, the argued advantages have been corroborated with experimental results, obtained from a high-bandwidth 2-D nanopositioning piezo-actuated stage with magnetoresistive position sensing.

ACKNOWLEDGEMENTS

The authors would like to thank all their colleagues at the University of Patras and at IBM Zurich Research Laboratory. In particular V. Kartik for the design of the nanopositioner, U. Egger and W. Haeberle for their invaluable technical assistance, and T. Tuma for all the fruitful technical conversations on the subject. They would also like to thank H. Pozidis and E. Eleftheriou for their support to this project.

REFERENCES

- Bhushan, B. (2004). *Handbook of Nanotechnology*. Springer Verlag, Germany.
- Daughton, J. (2003). Spin-dependent sensors. Proceedings of the IEEE, 91(5), pp. 681–686.
- Devasia, S., Eleftheriou, E., and Moheimani, S.O.R. (2007). A survey of control issues in nanopositioning. *IEEE Trans. on Control System Technology*, 15(5).
- Kartik, V., Sebastian, A., Tuma, T., Sahoo, D., Pozidis, H., and Pantazi, A. (2010). High Speed Nanopositioner with Magneto Resistance-Based Position Sensing. 5th IFAC Symposium on Mechatronic Systems, Cambridge, Massachusetts.
- Kotsopoulos, A. and Antonakopoulos, T. (2010). Nanopositioning using the spiral of archimedes: The probe-based storage case. *Mechatronics*, 20(2), Elsevier.
- Kotsopoulos, A., Pantazi, A., and Antonakopoulos, T. (2010). Control for high speed archimedean spiral nanopositioning. The 17th IEEE International Conference on Electronics, Circuits, and Systems, ICECS, December 2010, Athens, Greece.
- Mahmood, I. and Moheimani, S. (2009). Fast Spiral-Scan Atomic Force Microscopy. *Nanotechnology* 20, 365503, IOP Publishing.
- Mahmood, I., Moheimani, S., and Bhikkaji, B. (2011). A New Scanning Method for Fast Atomic Force Microscopy. *IEEE Transactions on Nanotechnology*, 10(2).
- Mamun, A.A., Guo, G., and Bi, C. (2007). *Hard Disk Drive Mechatronics and Control*. CRC Press.
- Mishra, S., Coaplen, J., and Tomizuka, M. (2007). Precision positioning of wafer scanners. *IEEE Control Systems Magazine*, 27(4), pp. 2025.
- Pantazi, A., Sebastian, A., Antonakopoulos, T., Bächtold, P., Bonaccio, A.R., Bonan, J., Cherubini, G., Despont, M., DiPietro, R.A., Drechsler, U., Dürig, U., Gotsmann, B., Häberle, W., Hagleitner, C., Hedrick, J.L., Jubin, D., Knoll, A., Lantz, M., Pentarakis, J., Posidis, H., Pratt, R.C., Rothuizen, H., Stutz, R., Varsamou, M., Wiesmann, D., and Eleftheriou, E. (2008). Probe-based ultrahigh-density storage technology. *IBM J. Res. and Dev.*, 52(4/5), 493–511.
- Pantazi, A., Sebastian, A., Cherubini, G., Lantz, M., Rothuizen, H.P.H., and Eleftheriou, E. (2007). Control of MEMS-based scanning-probe data storage devices. *IEEE Transactions on Control System Technology*, 15(5).
- Sahoo, D., Sebastian, A., Haeberle, W., Pozidis, H., and Eleftheriou, E. (2011). Scanning probe microscopy based on magnetoresistive sensing. *Nanotechnology* 22, 145501, IOP Publishing.
- Sebastian, A., Pantazi, A., Pozidis, H., and Eleftheriou, E. (2008). Nanopositioning for probe-based data storage. *IEEE Control Systems Magazine*.
- Shibata, M., Yamashita, H., Uchihashi, T., Kandori, H., and Ando, T. (2010). High-speed atomic force microscopy shows dynamic molecular processes in photoactivated bacteriorhodopsin. *Nature Nanotechnology*, 5, pp. 208-212.
- Skogestad, S. and Postlethwaite, I. (2005). *Multivariable feedback control: analysis and design*. Wiley-Interscience, 2nd edition.